Title
STOCHASTIC NMR IMAGING: SPATIAL LOCALIZATION WITH OSCILLATING GRADIENTS

Authors
Roos, M.S.
Wong, S. T. S.

Publication Date
1989-06-01

LBL-27431
Preprint

Lawrence Berkeley Laboratory
UNIVERSITY OF CALIFORNIA

Submitted to Journal of Magnetic Resonance

Stochastic NMR Imaging: Spatial Localization with Oscillating Gradients

M.S. Roos and S.T.S. Wong

June 1989

Prepared for the U.S. Department of Energy under Contract Number DE-AC03-76SF00098.

DISCLAIMER

Stochastic NMR Imaging: Spatial Localization with Oscillating Gradients

M.S. Roos and S.T.S. Wong

Research Medicine and Radiation Biophysics Division

Lawrence Berkeley Laboratory

1 Cyclotron Road

Berkeley, CA 94720

Direct all correspondence to M.S. Roos, Mail Stop 55-121, at the address above. Telephone: (415) 486-4063.

Running header: Stochastic NMR Imaging

Abstract

A technique for spectroscopic imaging employing oscillating gradients for spatial encoding in conjunction with a stochastic rf excitation is proposed and analyzed. Localization functions are derived for a linearized model and compared with Bloch equation simulations. An implementation of the technique is described, and experimental point spread functions and a spectroscopic image (one spatial dimension and one chemical shift) are presented. Advantages of the technique are a large reduction in the peak rf power required relative to conventional pulse excitation and the elimination of switching transients through the use of oscillating gradients. Spectroscopic resolution and T_2 contrast may be varied by post processing a single experimental data set.

Introduction

Oscillating gradients can be used for rapid spatial encoding in NMR imaging (1). Chemical shift information is preserved, allowing spectroscopic imaging with rapid spatial encoding. This work extends previous analyses of imaging with oscillating gradients (2,3,4,5) to include stochastic rf excitation. The stochastic imaging experiment (6,7,8,9,10) consists of a sequence of rf pulses where the flip angles are a sample of a random or pseudo-random sequence. Stochastic NMR experiments have much larger rf duty cycles than conventional pulsed NMR, consequently the peak power requirements are several orders of magnitude lower. This reduction in peak rf power may be important for future in vivo spectroscopic imaging at fields of 4 T and above. Stochastic imaging is promising for detection of moieties with short T_2, because reduced rf pulse amplitude facilitates rapid receiver recovery and no delay for gradient switching is required. Stochastic encoding allows spectroscopic resolution and T_2 contrast to be varied by post-processing of a single experimental data set. T_1 contrast may be obtained by changing the excitation amplitude.

For this analysis, the excitation will be a discrete Gaussian white noise process. Experiments generally use maximum length sequences (MLS) for excitation. The auto-correlation functions of these pseudo-random sequences are similar to that of a white process. These excitations have been compared by Wong (11). With discrete excitation processes, one data point is sampled after every rf pulse in the presence of a B_0 gradient that varies sinusoidally throughout the experiment. The pulse sequence is shown in Fig. 1. To reconstruct an image, the cross correlation of the sampled signal with the product of the Gaussian white noise sequence and a phase demodulation kernel derived from the time-varying gradient waveform is estimated. This approach is a generalization of the weighted correlation reconstruction method, which is equivalent to all other linear reconstruction techniques with spatially invariant point spread functions (12). Because the excitation is a stochastic process, a statistical description of the image is appropriate even in the absence of noise. The expected value of the reconstructed image has the form of the spin distribution convolved with a localization function that is determined by the experimental parameters and the phase demodulation kernel.

Analysis of One Dimensional Imaging

A linearized model for the response of the magnetization to the rf excitation, valid in the limit of small flip angles, was used to obtain analytical expressions for the localization functions from several reconstruction schemes. The model is linear in the sense that the response to a sequence of rf pulses is taken to be the sum of the response to each pulse considered separately, and that the response is proportional to the amplitude of the excitation. The model is consistent with the Bloch equations in the limit of small flip angles. In terms of nonlinear systems theory, the model is the first term in the Volterra series representation of the response of the NMR spin system. The transverse magnetization

$m(x,t)$ may be described in terms of the excitation process $s(t)$ and the spin density $\rho(x)$:

$$m(x,t) = \rho(x) \int_0^\infty e^{-\tau/T_2} e^{-ixk(t,\tau)} s(t-\tau) d\tau.$$

In this model, the magnetization results from the action of a time-varying linear system on the excitation. Constants of proportionality have been suppressed to keep the notation compact. The effect of the magnetic field gradient $G(t)$ is included in $k(t,\tau)$:

$$k(t,\tau) = \gamma \int_{t-\tau}^{t} G(t')dt'.$$

A slightly different expression is obtained when $k(t,\tau)$ is separated into a difference

$$k(t,\tau) = \mathrm{k}(t) - \mathrm{k}(t-\tau),$$

where

$$\mathrm{k}(t) = \gamma \int_0^t G(t')dt'.$$

The transverse magnetization can then be written as

$$m(x,t) = \rho(x) e^{-ix\mathrm{k}(t)} \int_0^\infty e^{-\tau/T_2} e^{ix\mathrm{k}(t-\tau)} s(t-\tau) d\tau.$$

This represents a time invariant linear system (a one pole filter) with input $e^{-ix\mathrm{k}(t)} s(t)$ followed by modulation with $e^{ix\mathrm{k}(t)}$. In discrete form, this model may be simulated rapidly on a digital computer. The analytical results derived below were verified by simulations based on the linear model.

The received signal $y(t)$ is the spatial integral of the transverse magnetization:

$$y(t) = \int_{-\infty}^{\infty} m(x,t) dx. \qquad [1]$$

The estimate of the spin density is expressed by

$$\hat{\rho}(x',\eta) = \frac{1}{T} \int_0^T y(t)\, K(t,\eta,x')\, s^*(t-\eta) dt, \qquad [2]$$

where $K(t,\eta,x')$ is the phase demodulation kernel and T is the observation interval. A class of phase demodulation kernels is suggested by the linearized model:

$$K(t,\eta,x') = e^{ix'k(t,\eta)}w(t),$$

where

$$k(t,\eta) = \gamma \int_{t-\eta}^{t} G_m \cos\omega_m t' dt' \qquad [3]$$

and $w(t)$ is a weighting function. G_m and ω_m are the amplitude and angular frequency of the cosinusoidal gradient.

The expectation of this estimator can be written as a convolution

$$E\{\hat{\rho}(x',\eta)\} = \int_{-\infty}^{\infty} \rho(x)h(x'-x,\eta)dx,$$

in which $h(x,\eta)$ is the localization function. This result follows from substitution of Eq. [1] into Eq. [2] and the property $E[s(t-\tau)s^*(t-\eta)] = \delta(\tau-\eta)$. The localization function is

$$h(x,\eta) = \frac{1}{T}\int_0^T e^{-\eta/T_2+ik(t,\eta)x}w(t)dt. \qquad [4]$$

The choice of weighting function $w(t)$ controls the shape of the localization function. Three possible choices will be discussed below. For simplicity, the localization functions are not normalized; they produce scaled estimates of the spin density.

The localization function for a cosine gradient, Eq. [3], obtained by evaluating Eq. [4] and employing the series expansion

$$e^{iz\sin\theta} = \sum_{n=-\infty}^{\infty} e^{in\theta}J_n(z)$$

is

$$h(x,\eta) = \sum_p \sum_q J_p(\beta x)J_q(\beta x)e^{(-1/T_2+iq\omega_m)\eta}\frac{1}{T}\int_0^T e^{i(p-q)\omega_m t}w(t)dt \qquad [5]$$

where

$$\beta = \frac{\gamma G_m}{\omega_m}$$

and J_n is the Besselfunction of order n. The time lag of the cross correlation, η, is a free parameter that may be used to manipulate T_2 contrast and resolution. If the weighting function is periodic with period $2\pi/\omega_m$, it may be represented in a Fourier series expansion:

$$w(t) = \sum_{l=-\infty}^{\infty} a_l e^{il\omega_m t}. \qquad [6]$$

Using the orthogonality of the Fourier basis functions and the identity (13)

$$\sum_{m=-\infty}^{\infty} e^{im\alpha} J_m(u) J_{m+\nu}(u) = e^{i\nu(\pi-\alpha)/2} J_\nu(2u \sin(\alpha/2)),$$

it is evident that a non-zero Fourier coefficient of order l results in a term in J_l in the localization function. Thus

$$h(x,\eta) = \sum_l a_l e^{(-\eta/T_2 + il(\pi-\omega_m\eta)/2)} J_l(\xi x)$$

where

$$\xi = 2\beta \sin(\omega_m \eta/2).$$

For the case $w(t) = 1$, the time integral in Eq. [5] reduces to the Kroneker delta function δ_{pq}, and the localization function is

$$h(x,\eta) = e^{-\eta/T_2} J_0(\xi x).$$

Fig. 2a shows plots of the localization function for several values of η. The minimum half width of the main lobe is

$$\Delta x_{half} \approx \frac{1.5\omega_m}{\gamma G_m}.$$

for any choice of η.

The side lobes of the localization function can be reduced by including harmonics of the gradient frequency in the demodulation kernel, allowing synthesis of a localization

function from a series of Bessel functions of increasing order. For example, the weighting function

$$w(t) = (1 + e^{i2\omega_m t})/2$$

yields

$$h(x,\eta) = \frac{e^{-\eta/T_2}}{2}\left[J_0(\xi x) - e^{-i\omega_m \eta} J_2(\xi x)\right].$$

Fig. 2b shows plots of this localization function, varying η. The side lobes are much smaller than with the simple weighting function $w(t) = 1$. Applying the recursion relation for Bessel functions, $J_2(z) + J_0(z) = (2/z)J_1(z)$, this expression reduces to

$$h(x) = e^{-\eta/T_2} jinc(2\gamma G_m x/\omega_m) = e^{-\eta/T_2}\frac{J_1(2\gamma G_m x/\omega_m)}{2\gamma G_m x/\omega_m}$$

when $\eta = \pi/\omega_m$.

Shenberg (2) has demonstrated that a localization function decreasing as $|x|^{-(L+1/2)}$ can be synthesized from a linear combination of even-order Bessel functions up to order L, which are generated by a weighting function of the form

$$w(t) = \sum_{l=0}^{L} a_p e^{i2l\omega_m t}.$$

Another approach to selecting the coefficients a_l is to compensate for the variation of sample point density in k-space caused by the cosinusoidal gradient (12). In this case $w(t) = |\cos(\omega_m t)|$. The localization function calculated from the first 5 terms of the Fourier series expansion of $|\cos(\omega_m t)|$ is shown in Fig. 2c.

Localization functions with reduced sidelobes may also be synthesized by combining a range of correlation delays. Integrating over N periods of the gradient, Eq. [5] becomes

$$h(x) = \sum_p \sum_q J_p(\beta x) J_q(\beta x)\frac{1}{T}\int_0^T e^{i(p-q)\omega_m t} w(t)dt \int_0^{2\pi N/\omega_m} e^{(-1/T_2 + iq\omega_m)\eta} d\eta. \qquad [7]$$

If the integration time is long compared with the memory of the system ($2\pi N/\omega_m \gg T_2$), the localization function approaches

$$h(x) = \sum_p \sum_q J_p(\beta x) J_q(\beta x) \frac{1}{T} \int_0^T e^{i(p-q)\omega_m t} w(t) dt \left[\frac{T_2}{1 - iq\omega_m T_2} \right].$$

The terms in the summation over q are small for $|q| \neq 0$ provided that $T_2 \gg 1/\omega_m$. In this case

$$h(x) = T_2 J_0(\beta x) \sum_p J_p(\beta x) \frac{1}{T} \int_0^T e^{ip\omega_m t} w(t) dt.$$

Thus integrating over η results in a factor of $T_2 J_0$ in the localization function. As above, the Fourier series of $w(t)$ determines the rest of the localization function. For periodic weighting functions, the Fourier series of the weighting function, Eq. [6], may be employed, yielding

$$h(x) = T_2 J_0(\beta x) \sum_{l=-\infty}^{\infty} a_l J_l(\beta x).$$

For $w(t) = 1$, the localization function is

$$h(x) = T_2 J_0^2(\beta x).$$

This localization function is illustrated in Fig. 3. The half width of the main lobe is

$$\Delta x_{half} \approx \frac{2.2\omega_m}{\gamma G_m}.$$

As expected, some resolution has been traded for side lobe reduction. Localization functions corresponding to the other weighting functions discussed above are also shown in Fig. 3. The quantity $\gamma G_m x/\omega_m$ is similar to the modulation index in the theory of frequency modulated signals, and determines the rate at which the side bands decrease in the spectrum of the received signal.

Spectroscopic Imaging

The stochastic imaging experiment may be applied without modification to systems with multiple chemical shifts, provided that the gradient modulation frequency is greater than the range of shifts present. The method is also applicable to imaging in an inhomogeneous magnetic field.

Including chemical shift, σ, the transverse magnetization is

$$m(x,\sigma,t) = \rho(x,\sigma)e^{-ix\mathbf{k}(t)} \int_0^\infty e^{(-1/T_2+i\sigma)\tau} e^{ix\mathbf{k}(t-\tau)} s(t-\tau)d\tau.$$

The expectation of the spin density estimator will be

$$E\{\hat{\rho}(x',\eta)\} = \int_{-\infty}^{\infty}\int_{-\infty}^{\infty} \rho(x,\sigma)e^{-i\sigma\eta}h(x'-x,\eta)dxd\sigma, \qquad [8]$$

where an integral over σ has been included. Taking the Fourier transform (over η) produces a new estimator, $\hat{\rho}(x',\sigma')$, of the two dimensional spin density in space and chemical shift. This estimate may be written in terms of a two dimensional localization function:

$$E\hat{\rho}(x',\sigma') = \int_{-\infty}^{\infty}\int_{-\infty}^{\infty} \rho(x,\sigma)h(x'-x,\sigma'-\sigma)dxd\sigma.$$

The new localization function is

$$h(x,\sigma) = \sum_p \sum_q J_p(\beta x)J_q(\beta x)\frac{1}{T}\int_0^T e^{i(p-q)\omega_m t}w(t)dt \int_0^{2\pi N/\omega_m} e^{[-1/T_2+i(q\omega_m-\sigma)]\eta}d\eta. \qquad [9]$$

If the transform is sufficiently long that $2\pi N/\omega_m \gg T_2$,

$$h(x,\sigma) = \sum_p \sum_q J_p(\beta x)J_q(\beta x)\frac{1}{T}\int_0^T e^{i(p-q)\omega_m t}w(t)dt \left[\frac{T_2}{1+i(\sigma-q\omega_m)T_2}\right].$$

Thus the desired spectrum has the expected Lorentzian shape but is replicated at multiples of the gradient modulation frequency ω_m, as is typical of frequency modulated systems. The spectrum may be easily extracted by filtering as long as the replicated spectra do

not overlap, that is, when the modulation frequency is greater than the chemical shift bandwidth. The baseband spectrum will have the localization function

$$h(x,\sigma) = J_0(\beta x)\sum_p \sum_q J_p(\beta x)\frac{1}{T}\int_0^T e^{i(p-q)\omega_m t} w(t)dt \left[\frac{T_2}{1+i\sigma T_2}\right].$$

For periodic weighting functions and $T_2 \gg 1/\omega_m$, this can be expressed in terms of the Fourier coefficients a_l:

$$h(x,\sigma) = J_0(\beta x)\sum_l a_l J_l(\beta x)\left[\frac{T_2}{1+i\sigma T_2}\right].$$

The two dimensional localization function is seen to separate into a product of spatial and spectral localization functions. Spectroscopic resolution is not affected by the stochastic excitation or the localization gradients.

Comparison of Linearized Model and Numerical Bloch Equation Solution

As the power of a stochastic excitation is increased, the system response will increase up to a maximum and then decrease (saturation). The power of the observed signal as a function of excitation power may be easily predicted (11), and exhibits saturation similar to conventional pulsed NMR. The effect of the excitation power on the localization function was studied by comparing simulated data generated by the linearized model and a Bloch equation model with hard pulses. The reconstruction algorithms developed above were applied to this simulated data. The effect of the system nonlinearity on the shape of the localization function is negligible for excitation power up to that which yields the maximum response from the spin system. An example is shown in Fig. 4, along with the localization function for a very saturated system. Thus the results of the linearized analysis are directly applicable to the real system in the regime of practical interest.

Variance of the Density Estimator

Previous sections have focused on the expectation of the spin density estimator. Here the variance of $\hat{\rho}(x',\eta)$ due to the stochastic excitation is derived. This statistic is a measure of the accuracy of the estimator $\hat{\rho}(x',\eta)$ in the absence of measurement noise. The variance of may be written as the difference:

$$Var\{\hat{\rho}(x',\eta)\} = E\{|\hat{\rho}(x',\eta)|^2\} - [E\{\hat{\rho}(x',\eta)\}]^2.$$

From Eq. [1, 2] the mean square of $\hat{\rho}(x',\eta)$ is

$$\begin{aligned} E\{|\hat{\rho}(x',\eta)|^2\} \;=\; & \frac{1}{T^2}\int_{-\infty}^{\infty}\int_{-\infty}^{\infty}\int_0^T\int_0^T\int_0^{\infty}\int_0^{\infty} \rho(x_1)\rho(x_2)e^{-(\tau_1+\tau_2)/T_2}\, e^{-ix_1k(t_1,\tau_1)}\, e^{ix'k(t_1,\eta)} \\ & \times e^{ix_2k(t_2,\tau_2)}\, e^{-ix'k(t_2,\eta)}\, w(t_1)w^*(t_2) \\ & \times E\{s(t_1-\tau_1)s^*(t_1-\eta)s^*(t_2-\tau_2)s(t_2-\eta)\}d\tau_1\, d\tau_2\, dt_1\, dt_2\, dx_1\, dx_2. \end{aligned} \qquad [10]$$

The excitation process must be specified in order to evaluate the expectation. Consider a complex process $s(t) = s_x(t) + s_y(t)$, where $s_x(t)$ and $s_x(t)$ are independent zero mean Gaussian processes with variance $\sigma^2/2$. Substituting expectation

$$E\{s(t_1-\tau_1)s^*(t_1-\eta)s^*(t_2-\tau_2)s(t_2-\eta)\} = \delta(\tau_1-\eta)\delta(\tau_2-\eta) + \delta(t_1-t_2)\delta(\tau_1-\tau_2)$$

into Eq. [10], it is easily demonstrated that the first product of delta functions yields $[E\{\hat{\rho}(x',\eta)\}]^2$. Thus

$$Var\{\hat{\rho}(x',\eta)\} = \frac{1}{T^2}\int_{-\infty}^{\infty}\int_{-\infty}^{\infty}\rho(x_1)\rho(x_2)\int_0^T\int_0^{\infty} e^{-2\tau/T_2}\, e^{-i(x_2-x_1)k(t,\tau)}|w(t)|^2 d\tau dt dx_1 dx_2.$$

This expression shows the important result that the variance of $\hat{\rho}(x',\eta)$ is independent of position and correlation lag (x' and η, respectively). It is bounded above,

$$Var\{\hat{\rho}(x',\eta)\} \le \frac{T_2}{2T^2}\int_0^T |w(t)|^2\, dt \left[\int_{-\infty}^{\infty}\rho(x)\, dx\right]^2,$$

and equality holds when $\rho(x) = \delta(x)$. Using Eq. [6] and the assumption that T is an integral multiple of the gradient period the above equation gives

$$Var\{\hat{\rho}(x',\eta)\} \leq \frac{T_2}{2T} \sum_{l=-\infty}^{\infty} |a_l|^2 \left[\int_{-\infty}^{\infty} \rho(x)\, dx\right]^2 .$$

This result shows that the variance of $\hat{\rho}(x',\eta)$ is inversely proportional to the observation time T. It is easily demonstrated that measurement noise (a complex process like $s(t)$, but independent of $s(t)$) will also contribute a variance inversely proportional to T.

Using Eq. [8] it can be shown that the variance of spin density estimator, $\hat{\rho}(x',\sigma')$, for the spectroscopic imaging experiment is similarly bounded:

$$Var\{\hat{\rho}(x',\sigma')\} \leq \frac{2\pi^2 N^2 T_2}{\omega_m^2 T} \sum_{l=-\infty}^{\infty} |a_l|^2 \left[\int_{-\infty}^{\infty}\int_{-\infty}^{\infty} \rho(x,\sigma)\, dx\, d\sigma\right]^2 . \qquad [11]$$

Again the variance goes to zero as T approaches infinity, and is independent of x' and σ. The variance of spin density estimators involving integration over η is a special case obtained by setting σ to 0 in Eq. [11].

Experimental Results

Experiments were conducted on a 0.5 T, 1 m bore imaging spectrometer equipped with a shift register circuit for generating 31 bit maximum length sequences (MLS). Sequences substantially shorter than the period of the generator were used for experiments. While such short sequences do not have the same autocorrelation functions as the entire MLS, the sequences of length 8192 points or more used here were observed to have no major spurious peaks in their autocorrelations. The MLS generator switched the transmitter phase between pulses, resulting in a train of rf pulses of equal flip angle but with sign determined by the MLS.

Fig. 5a is a one dimensional image of a vial of water. The diameter of the vial (2.5 cm) is smaller than the half-width of the localization function, so this image closely approximates the localization function corresponding to the weighting function $w(t) = 1$ and integration over η. The same data processed with the $w(t) = (1 + e^{i2\omega_m t})/2$, shown in Fig. 5b, demonstrates the reduction of side lobes with accompanying broadening of the main lobe. Fig. 6 is a spectroscopic image of a 100 ml beaker filled half with water doped with copper sulfate and half with oil, processed with $w(t) = 1$ and Fourier transformation. The materials are resolved in both position and chemical shift.

Discussion

The parameters to be selected in a stochastic imaging experiment are gradient strength and modulation frequency, sampling rate and flip angle. To avoid aliasing, the modulation frequency must be greater than the bandwidth of the spin system due to either field inhomogeneity or chemical shift (with no gradients applied). As demonstrated above, the gradient modulation frequency, gradient amplitude, and reconstruction method determine the localization function. The modulation frequency is fixed by the spin system bandwidth, consequently the gradient amplitude is chosen to achieve the desired spatial resolution. The received signal with oscillating gradients is not bandlimited, but Carson's rule (14) provides a working criterion for setting the sampling rate. In terms of the imaging experiment parameters, the approximate bandwidth, W, is

$$W = 2(\gamma G_m R + \omega_m),$$

where R is the greatest distance from the origin (zero crossing of the gradient) to a point within the object.

As examples reflecting on the practicality of the method, the chemical shift range (or minimum gradient modulation frequency) $\Delta\omega$, the effective signal bandwidth W, and the localization function half-width Δx_{half} are tabulated (Table 1) for several nuclei. The example is a R=10 cm object in a 4 T static field imaged with a 10 mT/m gradient. The data are processed to yield the localization function J_0^2. The modulation frequencies are in the range of 1 to 5 KHz, and sampling rates are below 100 KHz. ^{13}C presents the greatest challenge, as a large gradient amplitude will be required to produce a useful localization function, about 50 mT/m for a half width of less than 2 cm. Whether such oscillating gradients are realzable and safe must be carefully evaluated.

Imaging with stochastic excitation and oscillating gradients produces well characterized localization functions with side lobe amplitude controlled by post processing. Spectroscopic imaging may be accomplished at gradient strengths and frequencies that are readily attainable. Extension of the method to two and three spatial dimensions requires only the addition of orthogonal gradients that are not harmonically related.

Acknowledgements

This research was supported in part by the Whitaker Foundation and by the Director, Office of Health and Environmental Research, U.S. Department of Energy under Contract No. DE-AC03-76SF00098.

References

(1) A. Macovski. *Magn. Reson. Med.* **2**, 29–40 (1985).

(2) I. Shenberg and A. Macovski. *IEEE Trans. Med. Imag.* **4**, 144–152 (1985).

(3) I. Shenberg and A. Macovski. *IEEE Trans. Med. Imag.* **4**, 165–174 (1985).

(4) S.D. Rand and A. Macovski. *IEEE Trans. Med. Imag.* **6**, 346–355 (1987).

(5) S.J. Norton. *IEEE Trans. Med. Imag.* **6**, 21–31 (1987).

(6) B. Blümich. *J. Magn. Reson.* **60**, 37–45 (1984).

(7) B. Blümich and H. W. Spiess. *J. Magn. Reson.* **66**, 66–73 (1986).

(8) M. Bernardo Jr., D. Chaudhuri, X-R Liu, and P.C. Lauterbur. Hadamard zeugmatography using 3-D projection reconstruction. In *Book of Abstracts, Soc. Mag. Res. Med. Fourth Ann. Meeting*, pages 944–945, 1985.

(9) X-R Liu. "Stochastic NMR Zeugmatographic Imaging". PhD thesis, State Univ. of New York, Dec. 1985.

(10) D. Chaudhuri. "Hadamard Zeugmatography Using 3-D Projection Reconstruction". Master's thesis, State University of New York at Stony Brook, Aug. 1986.

(11) S. T-S Wong. "Discrete Analysis of Stochastic NMR". PhD thesis, University of California, Berkeley, Dec. 1988.

(12) A. Maeda, K. Sano, and T. Yokoyama. *IEEE Trans. Med. Imag.* **7**, 26–31 (1988).

(13) P.M. Morse and H. Feshbach. "Methods of Theoretical Physics". Volume 2, McGraw-Hill Book Company, Inc., 1953.

(14) F.G. Stremler. "Introduction to Commmunication Systems", pages 279–349. Addison-Wesley, 1982.

Table 1: Gradient modulation frequency, resolution, and signal bandwidth for spectroscopic imaging with time-varying gradients for a 10 cm object at 4.0 T with 10 mT/m gradient.

Nucleus	^1H	^{31}P	^{13}C
$\omega_m/2\pi = \Delta\omega/2\pi$ (10^3 Hz)	1.69	1.46	4.54
$W/2\pi$ (10^3 Hz)	88.5	37.3	30.4
Δx_{half} (cm)	0.87	1.87	9.33

Figure Captions

Figure 1: Pulse sequence for a one dimensional stochastic imaging experiment with sinusoidal gradient.

Figure 2: Plots of localization functions for three weighting functions: a) $w(t) = 1$, b) $w(t) = (1 + e^{i2\omega_m t})/2$ and c) $w(t) = |\cos(\omega_m t)|$. The imaging parameters are: 1 mT/m oscillating gradient at 381 Hz, and 105 μsec/sample. Three delays are plotted: $\eta = 0$, solid; $\eta = \pi/2\omega_m$, dashed; $\eta = \pi/\omega_m$. The delays cover one half of the period of the gradient.

Figure 3: Localization functions for the imaging parameters and the three weighting functions of Fig. 2, integrated over the correlation lag η. T_2 is 50 ms.

Figure 4: Comparison of linear model (solid line) and Bloch equation. The simulation used 65536 time samples, T_1 is 200 ms and T_2 is 50 ms. The imaging parameters are: 0.93 mT/m oscillating gradient at 381 Hz, and 105 μsec/sample. (integrated over 5 gradient cycles). The maximum response of the Bloch equation model occurs for an excitation process with RMS flip angle 3.6 degrees (dotted line). The localization function under extreme saturation, RMS flip angle of 20 degrees, (dashed line) illustrates the breakdown of the linear model at very large flip angles. Data are normalized to be equal to 1 at the origin.

Figure 5: Image of a 2.5 cm vial of water doped with copper sulfate, scaled such that the peak value is 1. The imaging parameters are the same as Fig. 4, but only 8192 samples were acquired. The solid line corresponds to the weighting function $w(t) = 1$ and the dotted line to $w(t) = (1 + e^{i2\omega_m t})/2$.

Figure 6: Spectroscopic image (arbitrary density units) of a 100 ml beaker containing equal

portions of oil and water doped with copper sulfate obtained with an oscillating gradient in the vertical direction. Imaging parameters are the same as Fig. 4 (65536 samples acquired). The image was processed with $w(t) = 1$. The first 1024 correlation values were Fourier transformed, and the 41 bins centered about the spectrometer reference frequency (0 Hz on the plot) were plotted.

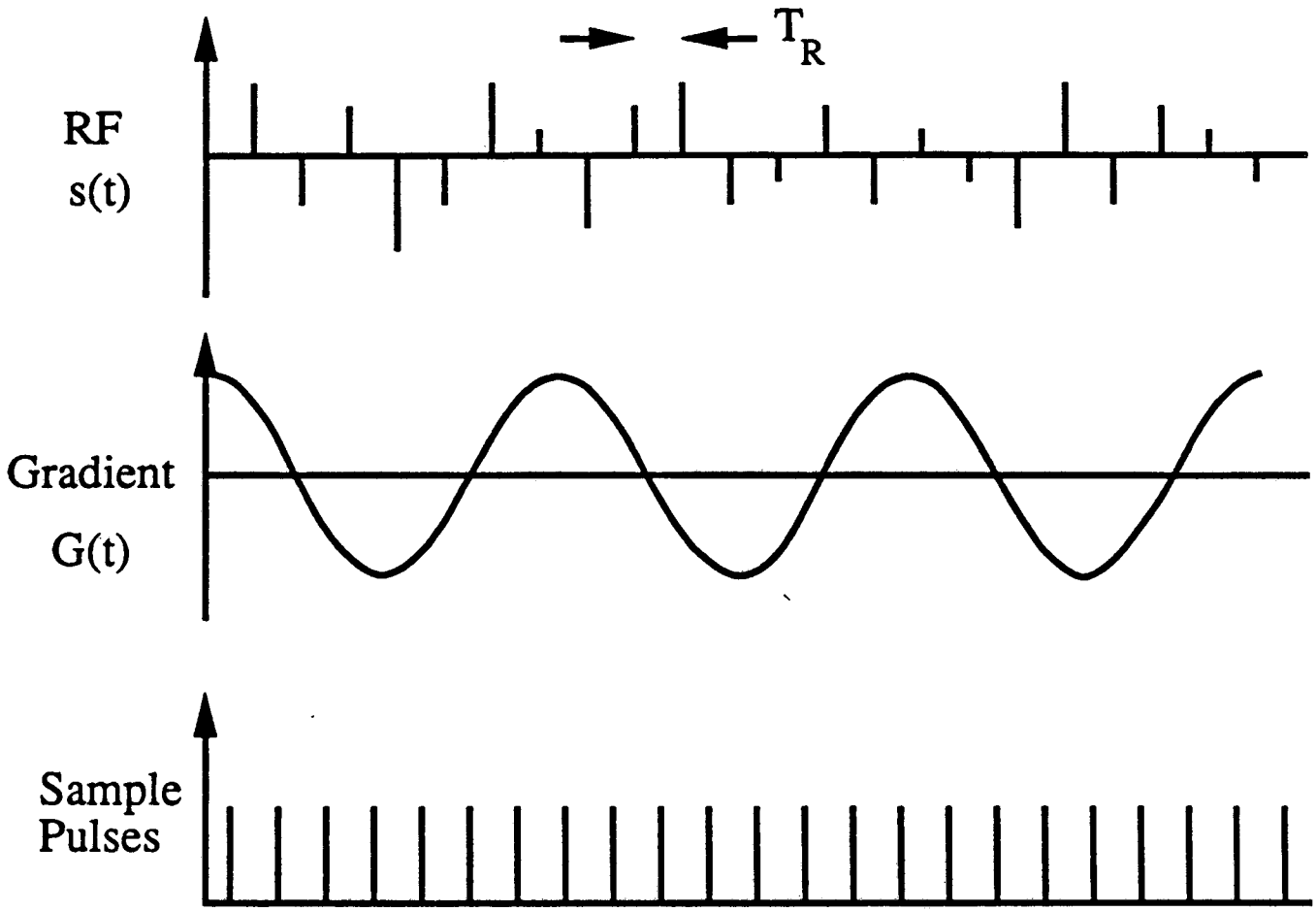

Fig. 1

(a)

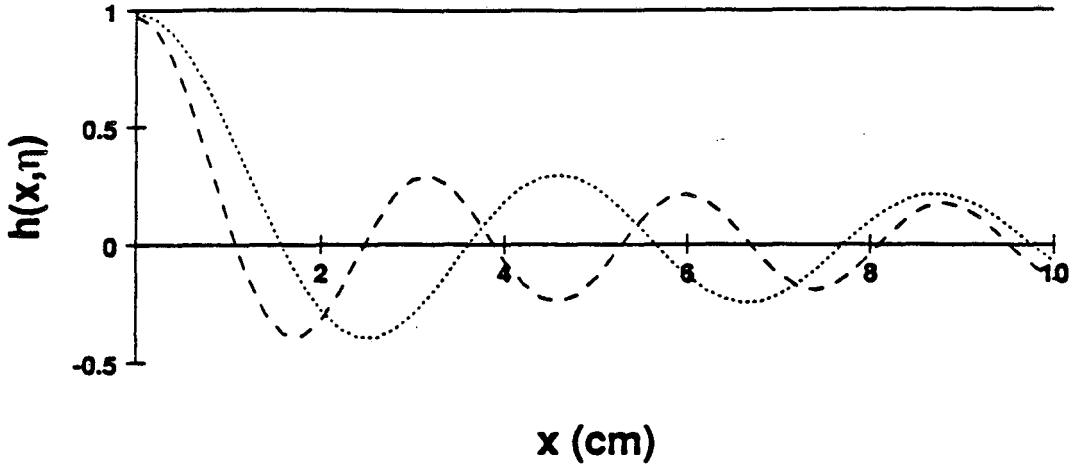
1
0.5
0
-0.5
2
4
6
8
10
h(x,η)
x (cm)

(b)

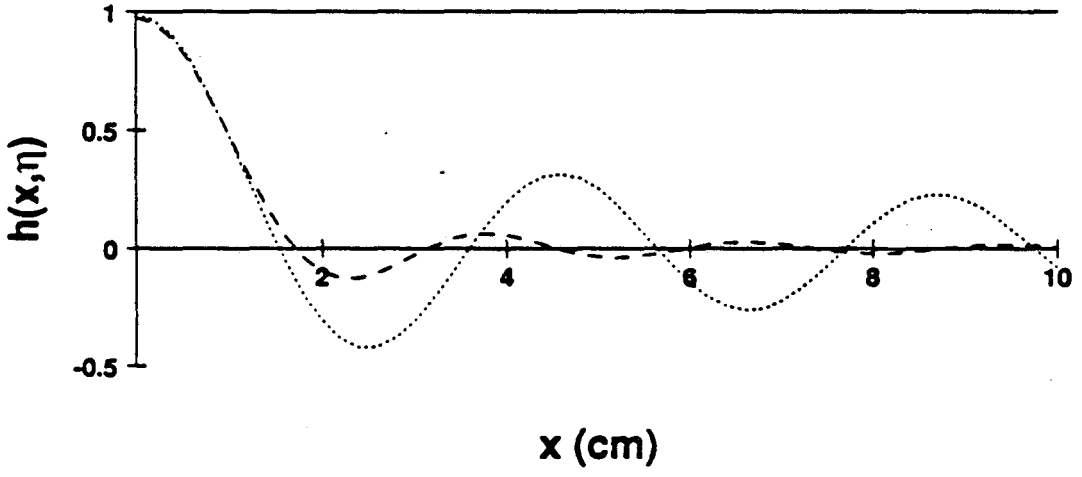
1
0.5
0
-0.5
2
4
6
8
10
h(x,η)
x (cm)

(c)

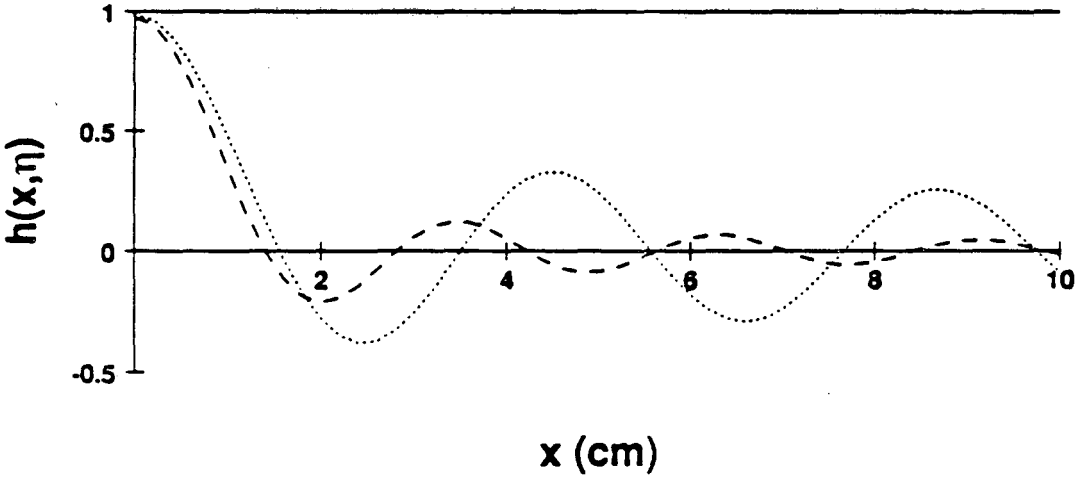
1
0.5
0
-0.5
2
4
6
8
10
h(x,η)
x (cm)

Fig. 2

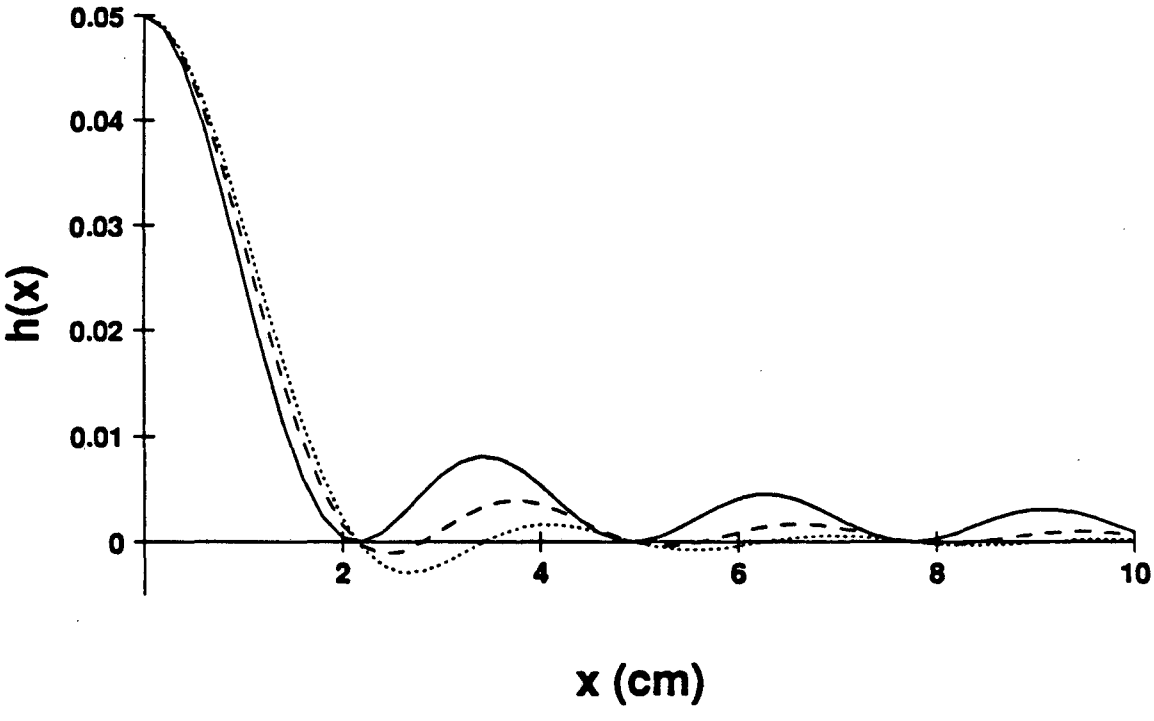

Fig. 3

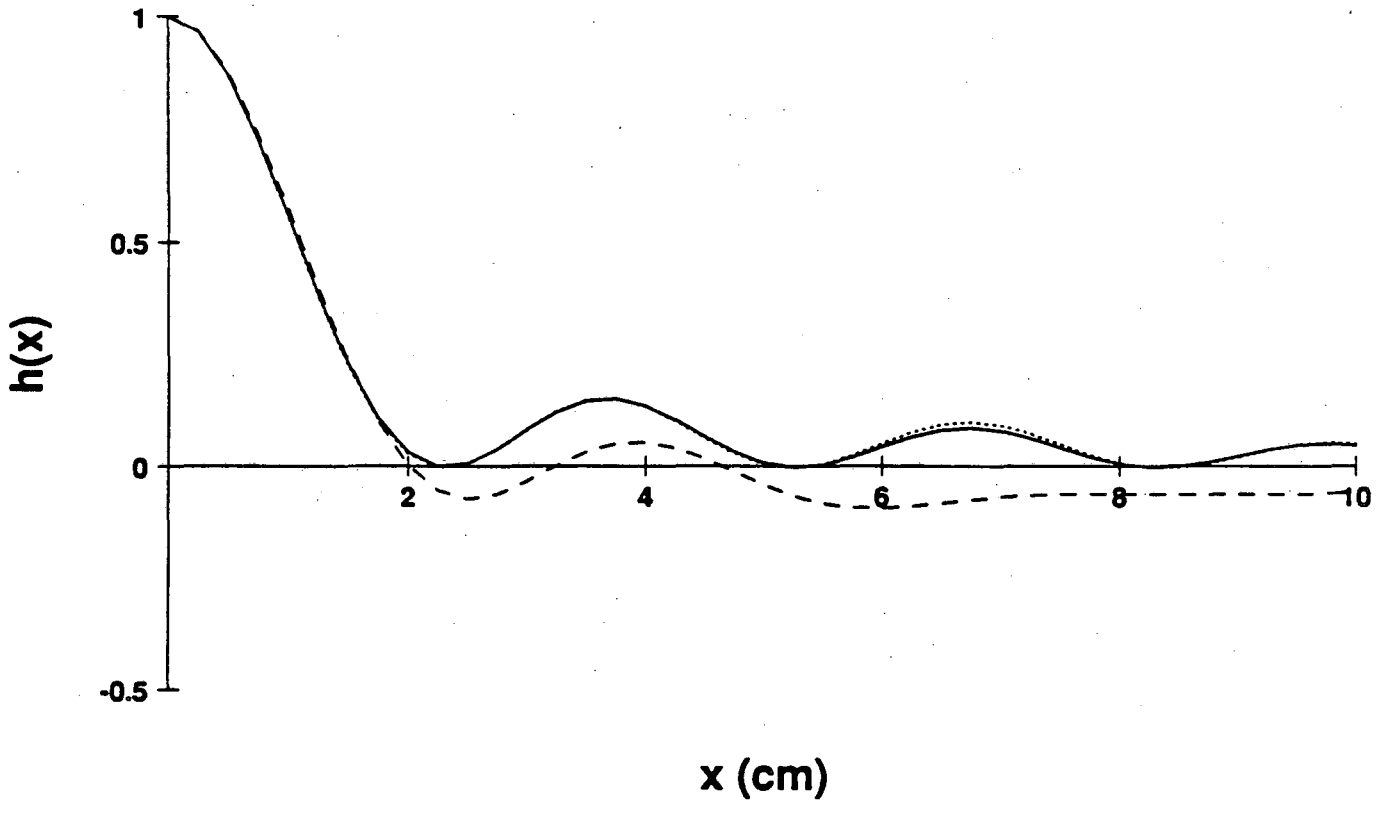

Fig. 4

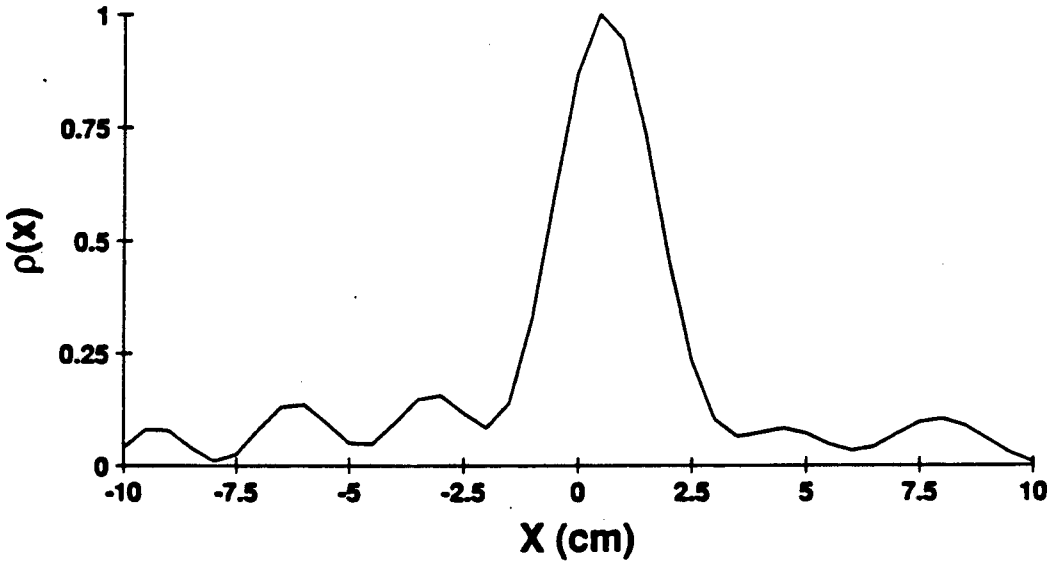
1
0.75
0.5
0.25
0
ρ(x)
-10
-7.5
-5
-2.5
0
2.5
5
7.5
10
X (cm)

(a)

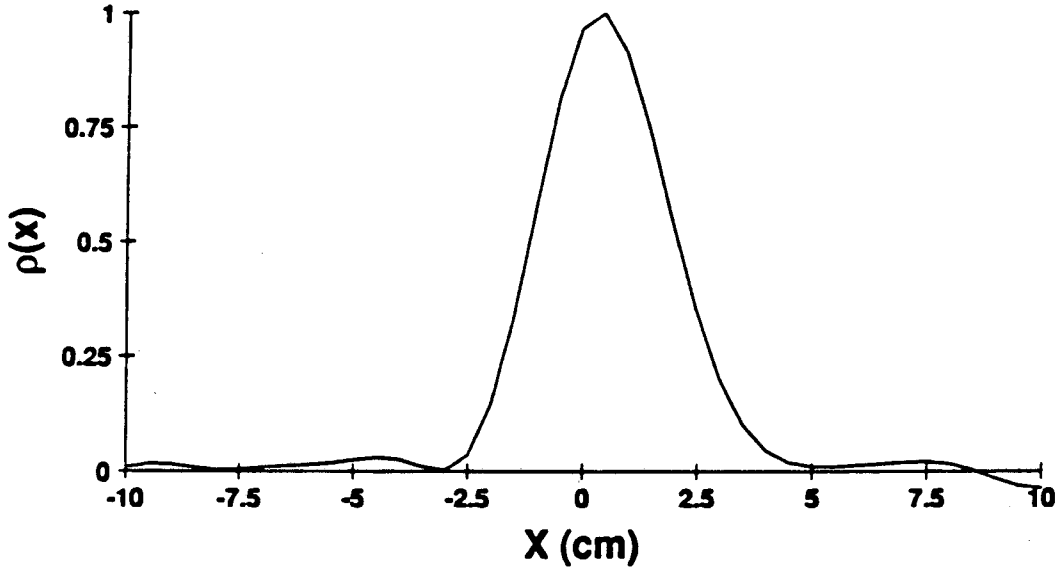
1
0.75
0.5
0.25
0
ρ(x)
-10
-7.5
-5
-2.5
0
2.5
5
7.5
10
X (cm)

(b)

Fig. 5

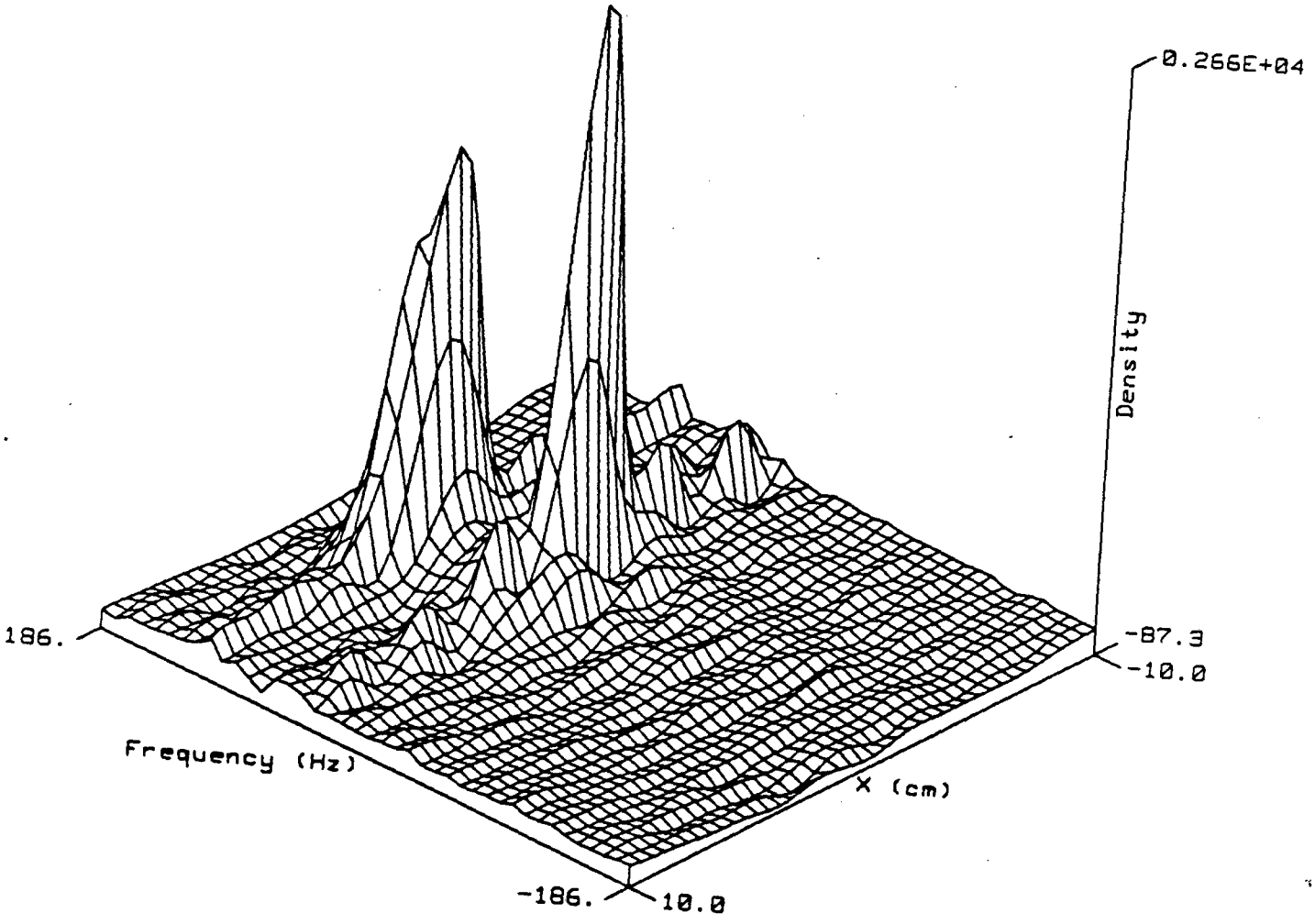

Fig. 6

LAWRENCE BERKELEY LABORATORY
TECHNICAL INFORMATION DEPARTMENT
1 CYCLOTRON ROAD
BERKELEY, CALIFORNIA 94720